Centrum voor Wiskunde en Informatica

REPORT*RAPPORT*

Solution of Time-dependent Advection-diffusion Problems with the Sparse-grid Combination Technique and a Rosenbrock Solve

B. Lastdrager, B. Koren, J.G. Verwer

Modelling, Analysis and Simulation (MAS)

MAS-R0025 September 30, 2000

Report MAS-R0025
ISSN 1386-3703

CWI
P.O. Box 94079
1090 GB Amsterdam
The Netherlands

Solution of Time-dependent Advection-diffusion Problems with the Sparse-grid Combination Technique and a Rosenbrock Solver

Boris Lastdrager, Barry Koren and Jan Verwer
CWI
P.O. Box 94079, 1090 GB Amsterdam, The Netherlands

ABSTRACT
In the current paper the efficiency of the sparse-grid combination technique applied to time-dependent advection-diffusion problems is investigated. For the time integration we employ a third-order Rosenbrock scheme implemented with adaptive step-size control and approximate matrix factorization. Two model problems are considered, a scalar 2D linear, constant-coefficient problem and a system of 2D nonlinear Burgers' equations. In short, the combination technique proved more efficient than a single grid approach for the simpler linear problem. For the Burgers' equations this gain in efficiency was only observed when one of the two solution components was set to zero, making the problem more grid-aligned.

2000 Mathematics Subject Classification: 65G99, 65M20, 65M55, 65L06, 76R99.
Keywords and Phrases: advection-diffusion problems, sparse grids, combination techniques, Rosenbrock methods, error analysis.
Note: This work was performed under a research contract with The Netherlands Organization for Scientific Research (NWO) and was carried out under CWI-projects MAS1.1 "Numerical Algorithms for Air Quality Modeling" and MAS2.1 "Computational Fluid Dynamics".

1. Introduction

In modern CFD codes accurate resolution of thin solution layers is still very time consuming. Especially for high Reynolds numbers many grid points are needed to resolve the very thin layers. The common remedy is to use adapted grids that have small cells near the layers and large cells elsewhere. In this paper we investigate another approach to resolve the thin layers, namely the sparse grid combination technique (CT) as introduced by Griebel, Schneider and Zenger [4].

The CT is attractive because, asymptotically, it can yield a smaller spatial error for a given complexity than a single grid approach (SG) can [14], [1]. Consider a problem of spatial dimension d that is solved on a single grid with spatial discretization of order p, i.e., on a single grid of mesh width h the spatial error is $O(h^p)$. On a single grid this problem would have a complexity $\sim h^{-d}$. With the CT a spatial error of order $O(h^p(\log h)^{d-1})$ can be obtained with a complexity $\sim h^{-1}(\log h)^{d-1}$, i.e., an asymptotically first-order complexity is obtained with only a slightly larger error than for the SG. Furthermore, the CT can be easily and efficiently implemented on a parallel computer, see [3].

In [9] we investigated the efficiency of the CT when applied to a pure advection equation and concluded that for a non-grid-aligned solution the CT does not perform very well (see [9] for a more complete report). In [11] this was also found for some elliptic PDEs. Note that in [5] the CT is also applied to a pure advection equation, but here the efficiency of the CT is not considered.

In practice, advection-diffusion problems are usually solved on boundary-fitted grids. The corresponding solutions are usually grid-aligned. In this paper we study model advection-diffusion problems having this type of solution.

An essential ingredient for a CT solver for time-dependent problems is an efficient time accurate integrator. We use a three-stage, third-order Rosenbrock method implemented with built-in step-size control and approximate matrix factorization. Without step-size control the method can be implemented as a two-stage scheme. It uses approximate matrix factorization to greatly speed up the

solution process, hence we call it factorized ROS3. In [7] the same factorized ROS3 has been used, independently from the current paper and without the CT.

As model problems we consider a scalar two-dimensional, constant-coefficient advection-diffusion equation and a system of two-dimensional Burgers' equations. To evaluate the efficiency of the CT we compare it with a straightforward SG approach.

2. The model problems

2.1 Model problem 1: The advection-diffusion equation

We consider the constant-coefficient advection-diffusion equation

$$u_t + u_x - \varepsilon\left(u_{xx} + u_{yy}\right) = 0 \tag{2.1}$$

on the spatial domain $[-1,1]\times[-1,1]$ and take $u(x,y,0) = 0$ as initial solution. As boundary conditions we impose

$$u(-1,y,t) = \begin{cases} 0, & y < 0 \\ \frac{1}{2}, & y = 0 \\ 1, & y > 0 \end{cases}, \quad u_y(x,\pm 1,t) = 0, \quad u(1,y,t) = 0.$$

For $\varepsilon = 10^{-2}$ the solution at $t = 1$ is shown in Fig. 1. It possesses a horizontal and a vertical grid-aligned solution layer. The thickness of both layers is proportional to $\sqrt{\varepsilon}$ as $\varepsilon \to 0$. For the steady state solution we have derived an exact expression in terms of a Fourier sum,

$$\begin{aligned} u(x,y) &= \frac{3/2}{\left(1 - e^{\frac{1}{\varepsilon}}\right)} e^{\frac{x}{\varepsilon}} \left(1 - e^{\frac{(1-x)}{\varepsilon}}\right) + \sum_{n=1}^{\infty} B_n(x) \cos\left(n\pi y\right), \\ B_n(x) &= \frac{2\sin\left(\frac{n\pi}{2}\right)/n\pi}{e^{2\sqrt{\frac{1}{4\varepsilon^2} + n^2\pi^2}} - 1} e^{\frac{x}{2\varepsilon}} \left(e^{x\sqrt{\frac{1}{4\varepsilon^2} + n^2\pi^2}} - e^{(2-x)\sqrt{\frac{1}{4\varepsilon^2} + n^2\pi^2}}\right), \end{aligned}$$

and have used this expression to confirm that our numerical method converges to the correct solution in the limit $t \to \infty$.

2.2 Model problem 2: Burgers' equations

The two-dimensional Burgers' equations

$$\begin{aligned} u_t &= -uu_x - vu_y + \varepsilon\left(u_{xx} + u_{yy}\right), \\ v_t &= -uv_x - vv_y + \varepsilon\left(v_{xx} + v_{yy}\right), \end{aligned}$$

are considered on the spatial domain $[-1,1]\times[-1,1]$. The boundary conditions we impose are

$$u(-1,y,t) = \begin{cases} 1 - 4(y - \frac{1}{2})^2, & y \geq 0 \\ 1 - 4(y + \frac{1}{2})^2, & y < 0 \end{cases}, \quad u(x,\pm 1,t) = 0, \quad u_x(1,y,t) = 0,$$

and

$$v(-1,y,t) = -0.35\sin\left(\frac{1}{2}\pi y\right), \quad v_y(x,\pm 1,t) = 0, \quad v_x(1,y,t) = 0.$$

As initial solutions we take

$$\begin{aligned} u(x,y,0) &= \begin{cases} 1 - 4(y - \frac{1}{2})^2, & y \geq 0 \\ 1 - 4(y + \frac{1}{2})^2, & y < 0 \end{cases}, \\ v(x,y,0) &= -0.35\sin\left(\frac{1}{2}\pi y\right). \end{aligned}$$

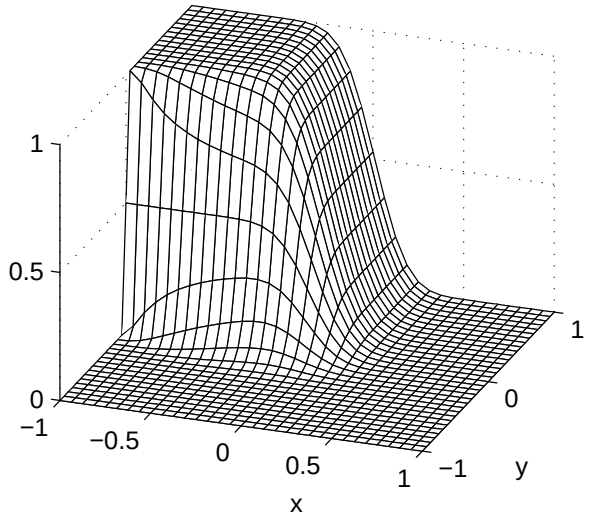

Figure 1: Solution of model problem 1 at $t = 1$ for $\epsilon = 0.01$

In Figures 2 and 3 the u and v components of the solution at $t = 3$ are shown for $\varepsilon = 10^{-2}$. The v component shows a sharpening from the sinusoidal inlet condition at $x = -1$ to a much steeper slope at the outflow boundary at $x = 1$. This is a grid-aligned phenomenon since near the outflow boundary the solution varies much stronger in y direction than in x direction. The u component shows a mixing of two jets. This phenomenon is not especially grid-aligned.

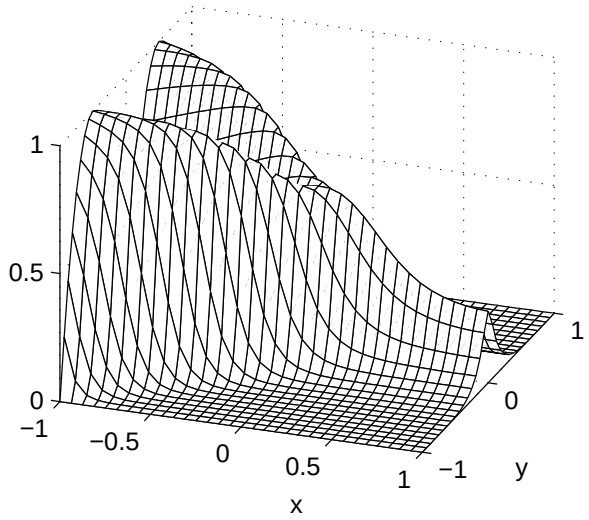

Figure 2: u-component of the solution of model problem 2 at $t = 3$ for $\epsilon = 0.01$

3. The sparse grid combination technique

In the CT several solutions on different grids are combined to get a solution which has the accuracy of a much finer grid. The two-dimensional CT is based on a grid of grids as shown in Fig. 4. Grids within the grid of grids are denoted by $\Omega^{l,m}$ where upper indices label the level of refinement relative

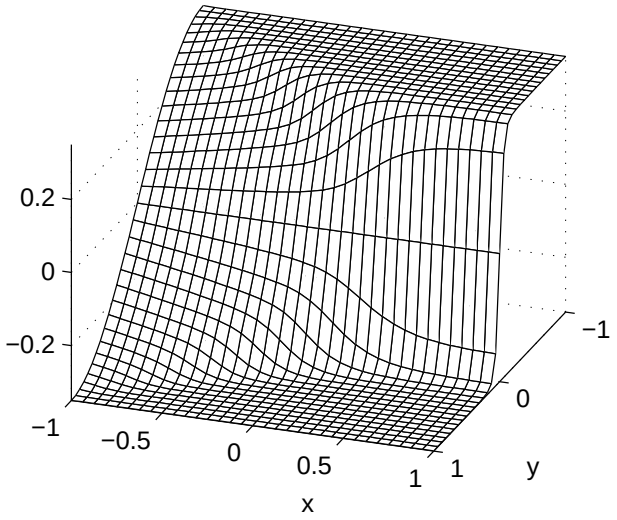

Figure 3: v-component of the solution of model problem 2 at $t = 3$ for $\epsilon = 0.01$

to the *root grid* $\Omega^{0,0}$. The mesh-widths in x and y direction of $\Omega^{l,m}$ are $h_x = 2^{-l}H$ and $h_y = 2^{-m}H$, where H is the mesh width of the uniform root grid $\Omega^{0,0}$. We denote the mesh width of the finest grid $\Omega^{N,N}$ by h. Note that h_x and h_y are dependent on the position (l, m) in the grid of grids while h is not.

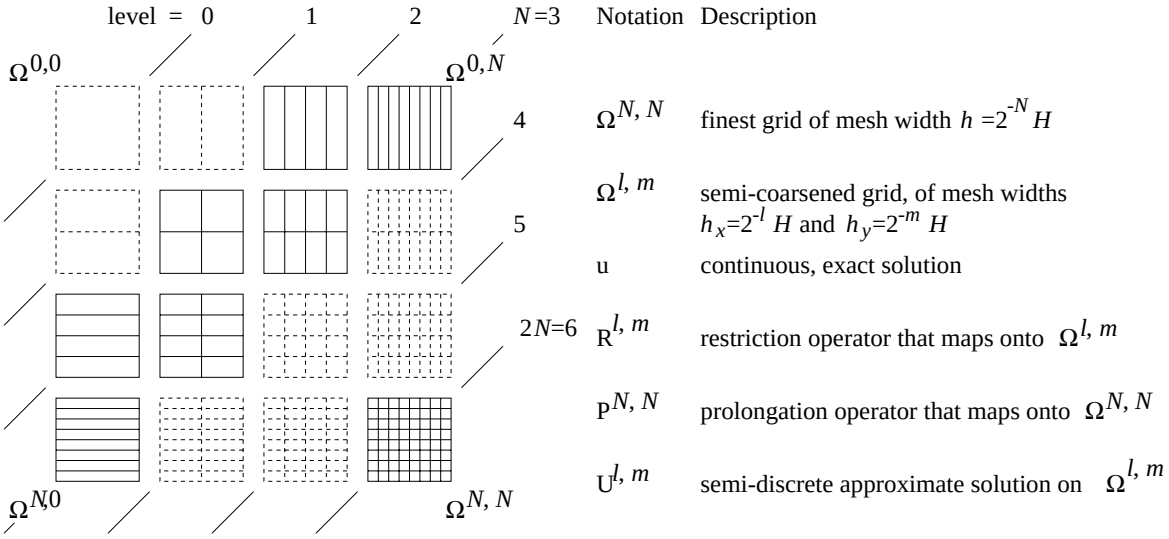

Figure 4: Grid of grids

In the time-dependent combination technique a given initial profile $u(x, y, 0)$ is restricted, by injection, onto the grids $\Omega^{N,0}$, $\Omega^{N-1,1}$, $\cdots$, $\Omega^{0,N}$ and onto $\Omega^{N-1,0}$, $\Omega^{N-2,1}$, $\cdots$, $\Omega^{0,N-1}$, see Fig. 4. The resulting coarse representations are then all evolved in time with our ROS3 time integrator. Then, at a chosen point in time, the coarse approximations are prolongated with q-th order interpolation onto the finest grid $\Omega^{N,N}$, where they are combined to obtain a more accurate solution. The notation is summarized in Fig. 4.

Considering the exact solution u, the combination technique, as introduced in [4], constructs a grid function $\widehat{u}^{N,N}$ on the finest grid $\Omega^{N,N}$ in the following manner,

$$\widehat{u}^{N,N} \equiv \sum_{l+m=N} P^{N,N} R^{l,m} u \; - \sum_{l+m=N-1} P^{N,N} R^{l,m} u.$$

The corresponding so-called *representation error* $r^{N,N}$ is

$$r^{N,N} \equiv \widehat{u}^{N,N} - R^{N,N} u. \tag{3.1}$$

Likewise, assuming exact time integration and considering semi-discrete solutions $U^{l,m}$, resulting from a spatial discretization, the combination technique constructs an approximate solution $\widehat{U}^{N,N}$ on the finest grid $\Omega^{N,N}$ from the coarse-grid approximate solutions according to

$$\widehat{U}^{N,N} = \sum_{l+m=N} P^{N,N} U^{l,m} - \sum_{l+m=N-1} P^{N,N} U^{l,m}. \tag{3.2}$$

Let $d^{l,m}$ denote the discretization error on grid $\Omega^{l,m}$, i.e.,

$$d^{l,m} \equiv U^{l,m} - R^{l,m} u. \tag{3.3}$$

The total error $e^{N,N} = \widehat{U}^{N,N} - R^{N,N} u$ present in $\widehat{U}^{N,N}$ is written as

$$e^{N,N} = r^{N,N} + \widehat{d}^{N,N},$$

where the *combined discretization* error $\widehat{d}^{N,N} = \widehat{U}^{N,N} - \widehat{u}^{N,N}$ is given by

$$\widehat{d}^{N,N} = \sum_{l+m=N} P^{N,N} d^{l,m} - \sum_{l+m=N-1} P^{N,N} d^{l,m}. \tag{3.4}$$

In [8] the representation error $r^{N,N}$ is analysed and in [10] an analysis is given of the combined discretization error $\widehat{d}^{N,N}$ for pure advection problems. In the next section we give similar results for the combined discretization error for our model problem 1, the linear, constant-coefficient advection-diffusion equation.

4. Spatial discretization errors

For the first test problem, the linear constant-coefficient advection-diffusion problem, we can derive an expansion in mesh widths for the spatial discretization error, as we did for the pure advection problem in [10]. Since essentially the same approach is used as in [10] we state only the results. We consider the error in the spatially discrete solution due to spatial discretization only, i.e., we assume here time integration to be exact. In (2.1) the diffusion terms are discretized with second-order central differences and the advection term is discretized with the third-order upwind biased discretization [6]. We only consider the error away from the boundaries, i.e., we neglect the influence of boundary conditions. When solved on a single grid with mesh widths h_x and h_y in x- and y-direction, the resulting spatial discretization error can then formally be expanded as

$$\begin{aligned}
d(x,y,t) &= \sum_{i=1}^{\infty} \frac{(-tE_{adv} - tE_{diff})^i}{i!} u(x,y,t), \\
E_{adv} &= \sum_{j=3}^{\infty} \frac{-(-2)^j + 3(-1)^j + 1}{3(j+1)!} h_x^j \partial_x^{j+1}, \\
E_{diff} &= \varepsilon \sum_{j=2}^{\infty} \frac{(-1)^j + 1}{(j+2)!} \left(h_x^j \partial_x^{j+2} + h_y^j \partial_y^{j+2} \right),
\end{aligned}$$

assuming that $u(x,y,t)$ is a C^∞ function. Neglecting $O(h_x^4)$ and $O(h_y^4)$ but including $O(h_x^2 h_y^2)$ for later comparison yields the following leading order expression

$$\begin{aligned} d(x,y,t) &= -\frac{t\varepsilon}{12}\left(h_x^2\partial_x^4 + h_y^2\partial_y^4\right)u(x,y,t) - \frac{t}{12}h_x^3\partial_x^4 u(x,y,t) \\ &\quad + \frac{t^2\varepsilon^2}{144}h_x^2 h_y^2 \partial_x^4\partial_y^4 u(x,y,t) + \mathcal{O}(h_x^4) + \mathcal{O}(h_y^4). \end{aligned}$$

Just as in [10] we use this result to determine the resulting spatial discretization error in the combined solution. It is given by

$$\begin{aligned} \widehat{d}(t) &= -\frac{t\varepsilon h^2}{12}\left(\partial_x^4 + \partial_y^4\right)u(t) - \frac{th^3}{12}\partial_x^4 u(t) \\ &\quad + \frac{t^2\varepsilon^2}{144}H^2h^2(1 - 3\log_2\frac{H}{h})\partial_x^4\partial_y^4 u(t) + \mathcal{O}(h^3\log_2\frac{1}{h}). \end{aligned} \tag{4.1}$$

The first error term is the usual leading error term on $\Omega^{N,N}$ coming from the diffusion operator. Similarly, the second term comes from the advection operator. The third term comes forth from the mixing of diffusion in x- and y-direction in the combination process. Since there is only advection in the x-direction, advection does not produce any additional error in the combined solution. In order for the CT to be effective the third term should be small compared to the first two terms. Asymptotically (as h and H tend to zero) this is clearly the case. In practice the asymptotics are not always strong enough for the third term, and higher mixed terms, to be negligible.

5. The Rosenbrock solver ROS3

We consider autonomous ODE systems of the form

$$\frac{dU}{dt} = f(U),$$

which are supposed to result from spatial discretization on one of our grids and seek a numerical approximation $U_n \approx U(t)$ at $t = t_n$. To obtain this approximation we apply a third-order consistent two-stage Rosenbrock method, ROS3 (also being used in [7]), which can be written as

$$\begin{aligned} U_{n+1} &= U_n + \frac{5}{4}k_1 + \frac{3}{4}k_2, \\ (I - \gamma\tau A)k_1 &= \tau F(U_n), \\ (I - \gamma\tau A)k_2 &= \tau F(U_n + \frac{2}{3}k_1) - \frac{4}{3}k_1, \end{aligned}$$

where $\tau = t_{n+1} - t_n$ is the step size and A is the Jacobian matrix $f'(U_n)$ or an $O(\tau)$ approximation thereof. This scheme is a variation to the scheme ROS2 as presented in [13] and belongs to a family of schemes discussed on p. 233 of [2]. Its stability function is

$$R(z) = \frac{1 + (1-2\gamma)z + (\frac{1}{2} - 2\gamma + \gamma^2)z^2}{(1-\gamma z)^2},$$

which shows that the scheme is A-stable if and only if $\gamma \geq 1/4$. The scheme is third-order accurate provided A is an $O(\tau)$ approximation of the Jacobian matrix and $\gamma = 1/2 + \sqrt{3}/6$. Note that this specific γ yields A-stability. Because our spatially discrete problems are stiff due to the diffusion term, A-stability is a desirable property.

5.1 Factorization

Since the ROS3 scheme remains of third-order for any $O(\tau)$ perturbation to $A = f'(U_n)$, we can split A as $A = A_1 + A_2$ and use

$$\begin{aligned} U_{n+1} &= U_n + \frac{5}{4}k_1 + \frac{3}{4}k_2, \\ (I - \gamma\tau A_1)(I - \gamma\tau A_2)k_1 &= \tau F(U_n), \\ (I - \gamma\tau A_1)(I - \gamma\tau A_2)k_2 &= \tau F(U_n + \frac{2}{3}k_1) - \frac{4}{3}k_1. \end{aligned}$$

The latter, factorized ROS3 scheme, is still of third-order since

$$(I - \gamma\tau A_1)(I - \gamma\tau A_2) = I - \gamma\tau(A - \gamma\tau A_1 A_2).$$

In the current work we use directional factorization to separate the horizontal and vertical coupling such that A_1 only couples unknowns in the horizontal direction and A_2 only couples unknowns in the vertical direction. This leads to enormous savings in required computational work since it reduces the two-dimensional linear algebra to one-dimensional linear algebra.

Without factorization, spatial discretization leads to pq coupled linear algebraic equations for the Rosenbrock vectors k_1 and k_2 where p is the number of unknowns in horizontal direction and q the number in vertical direction. With factorization, we have p sets of q coupled equations and q sets of p coupled equations for k_1 and likewise for k_2. This is a clear advantage of factorization since p sets of q coupled equations are solved much faster than one set of pq coupled equations. Another benefit of directional factorization is that the resulting sets of equations have band diagonal matrices and can therefore be solved very efficiently by means of LU decomposition.

In [7] it has been proven that a similar property as A-stability holds for the factorized ROS3 scheme. For our model problems this means that we have unconditional stability in the sense of Fourier-Von Neumann. Finally it should be noted that the above approximate matrix factorization is well known in the numeric PDE literature, see [7] for some references.

5.2 Time step size control

In our implementation of ROS3 we compute another auxiliary vector, k_3, to obtain an estimate for the local time error. The corresponding extra auxiliary equation is

$$(I - \gamma\tau A_1)(I - \gamma\tau A_2)k_3 = \tau F(U_{n+1}) + \frac{24\gamma^2 - 9\gamma - 1}{6\gamma(1 - 2\gamma)}k_1 + \frac{3\gamma - 1}{2\gamma(1 - 2\gamma)}k_2.$$

Our error estimate is

$$\begin{aligned} E_{est} &= -\frac{6\gamma^2 - 1}{6\gamma(1 - 2\gamma)}k_1 + \frac{6\gamma^2 - 6\gamma + 1}{2\gamma(1 - 2\gamma)}k_2 - k_3 \\ &= \frac{1}{6}\tau^3\frac{d^3c}{ct^3} + O(\tau^4), \end{aligned}$$

which is the last term in the Taylor expansion of the updated solution that our scheme still handles correctly. We strive for an equidistribution of errors, i.e., we attempt to keep E_{est}, measured in the L_1 norm, fixed at some tolerance Tol during the integration. To achieve this we adjust the step size τ according to

$$\tau_{new} = 0.8\tau_{old}\left(\frac{Tol}{\|E_{est}\|_1}\right)^{1/3}.$$

Solution updates are only performed when $\|E_{est}\|_1 \leq Tol$ at the new time level, otherwise the update is computed again with a smaller step size. The factor 0.8 is a safety factor and serves to avoid

excessive numbers of rejected updates. In our implementation the ratio τ_{new}/τ_{old} was kept bounded between 0.1 and 10.

Now consider the global time error e_n at time level t_n, i.e., the difference between the computed solution at time level t_n and the exact solution at the same time level. This error is in fact proportional to the tolerance Tol that we imposed, i.e.,

$$e_n \sim Tol.$$

This property of tolerance proportionality follows from [12], p. 350, when we identify our scheme as an XEPS scheme, i.e., an error per step control with local extrapolation. The proportionality between the imposed tolerance and the global time error is a nice property since it allows the user to control the global error in a very direct manner.

5.3 Numerical illustration of factorized ROS3

Figure 5 displays the integration history for the Burgers' equations solved up to $t = 3$ on a single 33×33 spatial grid with $Tol = 10^{-3}$. The step size τ is shown in the left graph and the error estimate $\|E_{est}\|_1$ in the right graph. We start with an initial step size $\tau = 10^{-2}$ which turns out to be somewhat too small for the imposed tolerance value. As the integration progresses larger step sizes are permissible. In the intermediate stage of the integration the step size remains almost constant. Finally, as the solution approaches steady state the size of the allowed step size quickly grows. During the integration the step size control keeps the error estimate $\|E_{est}\|_1$ at a nearly constant level, as can be seen from Fig. 5.

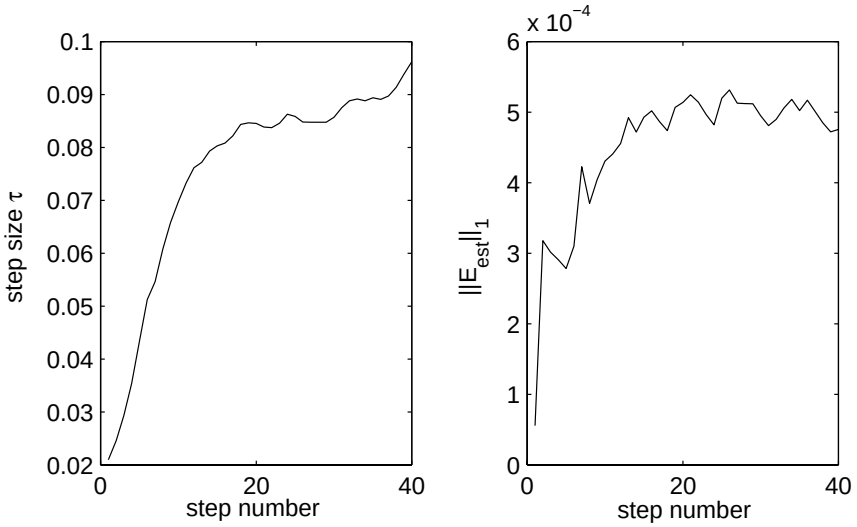

Figure 5: Integration history of model problem 2

In Table 1 the ratio of maximal global time errors E_{Tol} is shown for solutions with tolerance Tol and tolerance $Tol/2$ as a function of the tolerance. The time errors were estimated by subtracting a reference solution obtained with $Tol = 10^{-8}$. As the tolerance, and hence the step size, gets smaller we see that the ratio approaches 2, which confirms that the global time error is proportional to the imposed tolerance.

6. Results

In this section the CT is compared with the standard SG approach. Both are implemented with the same spatial discretization, i.e., second-order central discretization for the diffusion operator and third-order upwind-biased discretization for the advection part. The Neumann condition on the outflow

Tol	$L_\infty(E_{Tol})/L_\infty(E_{Tol/2})$
10^{-3}	1.748
10^{-4}	1.597
10^{-5}	1.878
10^{-6}	1.973

Table 1: Ratio of global time errors for model problem 2

boundary in model problem 1 is only imposed on the diffusion operator to avoid spurious reflections at that boundary.

6.1 Validation of the sparse grid error expression
In Fig. 6 a numerical illustration of the sparse grid error behaviour is given. Spatial errors are shown for solutions of (2.1) with initial profile

$$u(x, y, 0) = e^{-16(x^2+y^2)},$$

integrated up to $t = 0.25$, with $\varepsilon = 0.05$ and zero Dirichlet boundary conditions. A sparse grid with $N = 5$, i.e., containing 11 semi-coarsened grids, was used. The top row of Fig. 6 corresponds to solutions obtained with a root mesh width $H = 1/2$, the bottom row corresponds to $H = 1/8$. The errors in the left column were obtained numerically, i.e., by subtracting a reference solution obtained on a finer grid ($N = 5$, $H = 1/32$). The errors in the right column are predictions according to (4.1) where the derivatives of the solution were replaced by numerical differences of the reference solution.

The errors in the top row show oscillatory behaviour that is due to the third term in (4.1), i.e., the term due to combination. This behaviour is absent in the lower row. Here the third term, which is proportional to H^2, is negligible due to the smaller $H = 1/8$. The error prediction (4.1) illustrated in the right column clearly matches this transition in error behaviour.

6.2 Model problem 1: the advection diffusion equation
In Fig. 7 the efficiency of the CT is compared with the SG when applied to the linear constant-coefficient advection-diffusion equation. Along the vertical axes the error is plotted, measured in the L_1 norm for the left column of graphs and in the L_∞ norm for the right column. Along the horizontal axes the computational work is plotted in terms of number of required cell updates. The graphs in the top, middle and bottom row correspond to $\varepsilon = 10^{-2}$, 10^{-3} and 10^{-5}, respectively.

We see that for all these ε the CT is more efficient than the SG when we consider the errors in the L_1 norm. Also, the gain in efficiency becomes larger as ε is decreased. This is expected since for small ε the grid-aligned advection becomes more dominant rendering the test case more grid-aligned and hence better suited to the CT. For $\varepsilon = 10^{-3}$ and 10^{-5} the same holds for the L_∞ norm. For $\varepsilon = 10^{-2}$ the CT does not perform well when measured in the L_∞ norm. Examination of the corresponding spatial error distribution shows that the maximum error occurs near the discontinuity in the inlet condition. The mixed derivative u_{xxyy} is large near this discontinuity leading, for large ε, to a large term $\varepsilon^2 u_{xxyy}$ present in the spatial error due to the CT. Hence it is to be expected that for relatively large ε the CT performs poorly locally near the discontinuity.

6.3 Model problem 2: Burgers' equations
In Fig. 8 again the CT and SG are compared in terms of efficiency, this time for the 2D Burgers' test case. In Fig. 8 the diffusion parameter is kept fixed at $\varepsilon = 10^{-2}$ since varying the diffusion parameter does not change the qualitative conclusions that can be drawn from this figure. The top row corresponds to the Burgers' test case as described in Section 2.2. For this test case it is clear that the CT does not perform very well relative to the SG, either when measured in L_1 norm or in L_∞

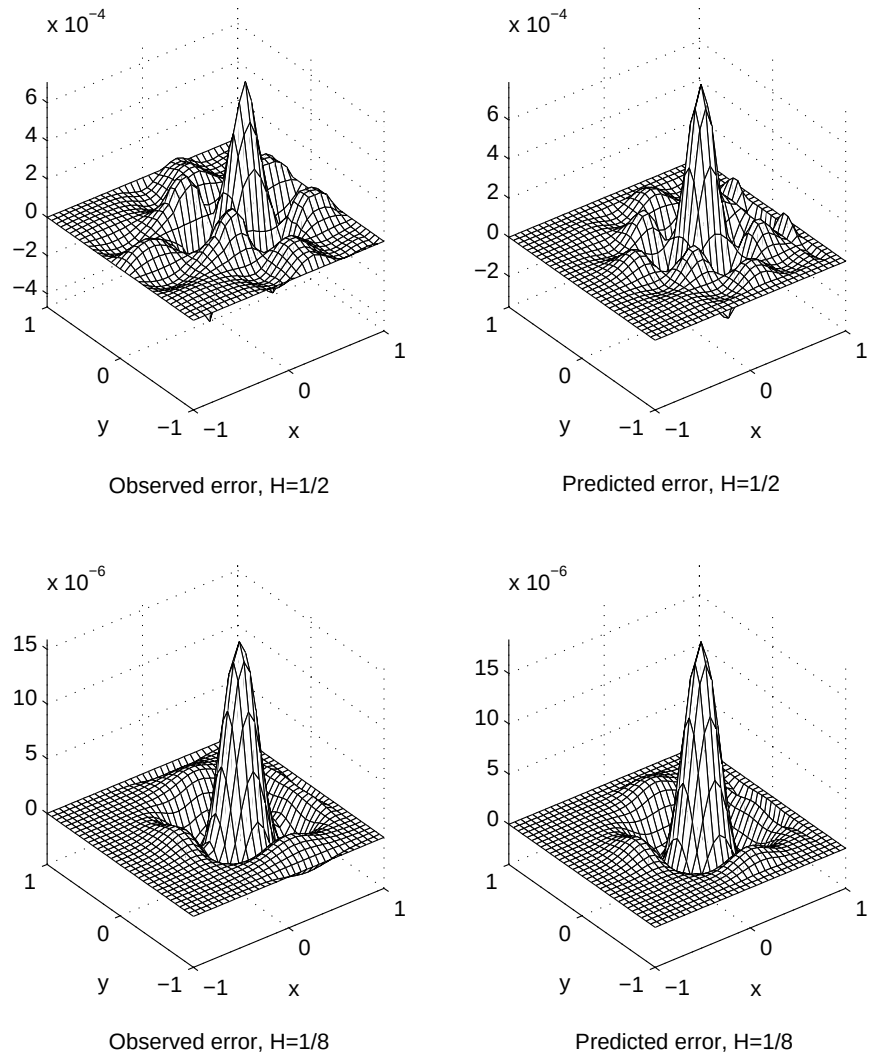

Figure 6: Spatial errors

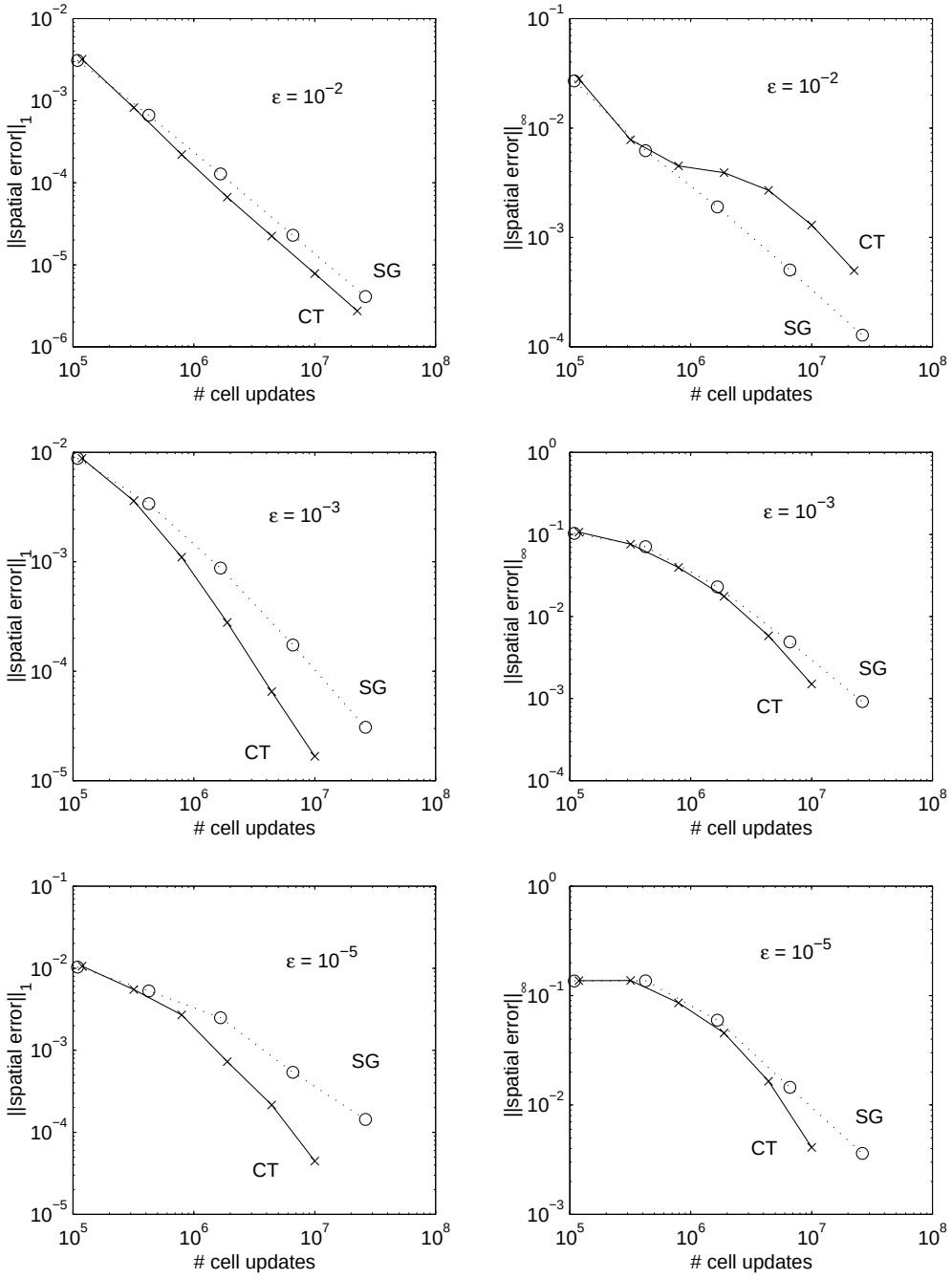

Figure 7: Efficiency comparisons for model problem 1

norm. It was expected that the Burgers' test case would be less well suited to the CT than the linear test case since the former is not as clearly grid-aligned.

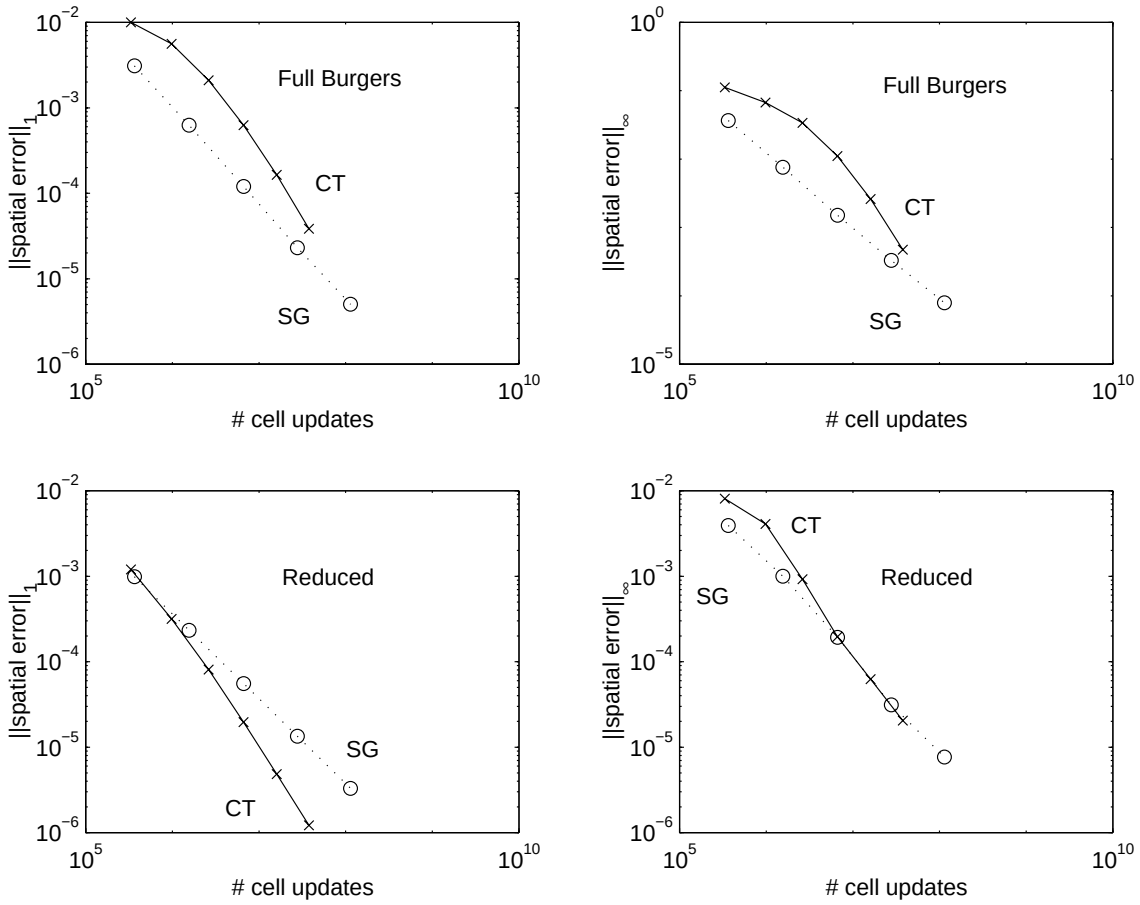

Figure 8: Efficiency comparisons for model problem 2

To see how the CT performs on the Burgers' test case when this is made more grid-aligned, we now take as initial condition $v = 0$ which guarantees that v remains zero. Furthermore we replace the parabolic inlet condition by

$$u(-1, y, t) = \begin{cases} \cos^2(y - \frac{1}{2}), & y \geq 0, \\ \cos^2(y + \frac{1}{2})^2, & y < 0. \end{cases}$$

This removes a strong peak in the error at $(x, y) = (-1, 0)$ which would otherwise dominate the error. The results for this reduced Burgers' test case are shown in the lower row of Fig. 8. Measured in the L_1 norm the CT outperforms a SG when applied to this reduced test case. Measured in the L_∞ norm this is still not the case, but at least the CT is comparable.

7. Conclusions

When applied to the simple grid-aligned, linear constant-coefficient test case the CT is clearly superior to the SG approach in terms of efficiency. Especially when the diffusion parameter ε is small, the linear test case is strongly grid-aligned and very well suited to the CT.

When applied to the 2D Burgers' test case, the CT does not perform so well. The CT does perform reasonably well for a reduced version of the Burgers' test case with advection in only one direction.

Based on these observations, our expectation that the CT is well suited to advection-diffusion problems that are strongly grid-aligned has been confirmed. But it seems that the CT is less suited to more general problems.

References

1. H. J. Bungartz, M. Griebel, D. Roschke and C. Zenger, *Pointwise convergence of the combination technique for the Laplace equation,* East-West J. Numer. Math., Vol. 2, No. 1, pp. 21-45, 1994.
2. K. Dekker and J. G. Verwer, *Stability of Runga-Kutta Methods for Stiff Nonlinear Differential Equations*, Elsevier North-Holland, Amsterdam, 1984.
3. M. Griebel, *The combination technique for the sparse grid solution of pde's on multiprocessor machines,* Parallel Processing Letters Vol. 2 No. 1 61-70, 1992.
4. M. Griebel, M. Schneider and C. Zenger, A combination technique for the solution of sparse grid problems, in: R. Beauwens and P. de Groen, eds., *Iterative Methods in Linear Algebra*, 263-281 (North-Holland, Amsterdam, 1992).
5. M. Griebel and G. Zumbusch, Adaptive sparse grids for hyperbolic conservation laws, in: W. Hackbusch and G. Wittum, eds., *Notes on Numerical Fluid Mechanics*, (Vieweg, Braunschweig, 1999).
6. B. Koren, 'A robust upwind discretization method for advection, diffusion and source terms', in: *Numerical Methods for Advection-Diffusion Problems* (C. B. Vreugdenhil and B. Koren, eds.), *Notes on Numerical Fluid Mechanics*, **45**, 117–138, Vieweg, Braunschweig (1993).
7. D. Lanser, J. G. Blom, J. G. Verwer, *Time integration of the shallow water equations in spherical geometry*, Report MAS-R0021, CWI, Amsterdam, 2000.
http://www.cwi.nl/static/publications/reports/MAS-2000.html
8. B. Lastdrager and B. Koren, *Error analysis for function representation by the sparse-grid combination technique*, Report MAS-R9823, CWI, Amsterdam 1998.
http://www.cwi.nl/static/publications/reports/MAS-1999.html
9. B. Lastdrager, B. Koren and J. G. Verwer, The sparse-grid combination technique applied to time-dependent advection problems, in: E. Dick, K. Riemslagh and J. Vierendeels, eds., Proceedings of the *Sixth European Multigrid Conference*, Gent, 1999, *Lecture Notes in Computational Science and Engineering*, **14**, 143–149, (Springer, Berlin, 2000).
10. B. Lastdrager, B. Koren and J. G. Verwer, *The sparse-grid combination technique applied to time-dependent advection problems*, Report MAS-R9930, CWI, Amsterdam, 1999.
http://www.cwi.nl/static/publications/reports/MAS-1999.html
11. U. Rüde, Multilevel, extrapolation and sparse grid methods, in: P. W. Hemker and P. Wesseling, eds., *Multigrid Methods*, **IV**, 281-294 (Birkhäuser, Basel, 1993).

12. L. F. Shampine, *Numerical Solution of Ordinary Differential Equations*, Chapman & Hall, New York, 1994.

13. J. G. Verwer, E. J. Spee, J. G. Blom and W. Hundsdorfer, *A second-order Rosenbrock method applied to photochemical dispersion problems*, SIAM J. Sci. Comput. Vol. 20, No. 4, pp. 1456-1480, 1999.

14. C. Zenger, Sparse grids, in: W. Hackbusch, ed., *Notes on Numerical Fluid Mechanics*, **31**, 241-251 (Vieweg, Braunschweig, 1991).